Ore Geology Reviews 84 (2017) 218–227

Contents lists available at ScienceDirect

Ore Geology Reviews

journal homepage: www.elsevier.com/locate/oregeo

Distance-gradient-based variogram and Kriging to evaluate cobalt-rich crust deposits on seamounts

Dewen Du [a,b,*], Chunjuan Wang [a], Xiaomeng Du [c], Shijuan Yan [a], Xiangwen Ren [a,b], Xuefa Shi [a,b], James R. Hein [d]

[a] First Institute of Oceanography, State Oceanic Administration, Qingdao 266061, China
[b] Evaluation and Detection Technology Laboratory of Marine Mineral Resources, Qingdao National Laboratory for Marine Science and Technology, Qingdao, 266061, China
[c] Statistics Department, University of Michigan, Ann Arbor, USA
[d] Pacific Coastal and Marine Science Center, United States Geological Survey, Santa Cruz, CA, USA

ARTICLE INFO

Article history:
Received 20 June 2016
Accepted 29 December 2016
Available online 18 January 2017

Keywords:
Seamounts
Cobalt-rich crust
Mineral resource evaluation
Geostatistics
Variogram

ABSTRACT

The spatial distribution of cobalt-rich crust thicknesses on seamounts is partly controlled by water depth and slope gradients. Conventional distance–direction-based variogram have not effectively expressed the spatial self-correlation or anisotropy of the thicknesses of cobalt-rich crusts. To estimate resources in cobalt-rich crusts on seamounts using geostatistics, we constructed a new variogram model to adapt to the spatial distribution of the thicknesses of the cobalt-rich crusts. In this model, we defined the data related to cobalt-rich crusts on seamounts as three-dimensional surface random variables, presented an experimental variogram process based on the distance–gradient or distance–"relative water depth," and provided a theoretical variogram model that follows this process. This method was demonstrated by the spatial estimation of the thicknesses of cobalt-rich crusts on a seamount, and the results indicated that the new variogram model reflects the spatial self-correlation of the thicknesses of cobalt-rich crusts well. Substituted into the Kriging equation, the new variogram model successfully estimated the spatial thickness distribution of these cobalt-rich crusts.

1. Introduction

Krige (1951) pioneered geostatistics, and later, Gel'fand and Jakubski (1961) defined a generalized random process that established a mathematical basis for geostatistics. Following the development and popularization of computers, David (1977) and Journel and Huijbregts (1978) extended the application of geostatistics to calculating mineral reserves. Since then, the geostatistical approach (Kriging for short) has become a widely used and effective method for mineral resource estimations and reserve calculations.

The essence of Kriging lies in the assignment of a weight coefficient to interpolations based on the self-correlation and geometric anisotropy of spatial variables. A variogram is a tool that expresses this self-correlation and the geometric anisotropy of spatial variables and provides a prior covariance matrix to execute the Kriging equation for spatial interpolation (Luenberger, 1969; Journel, 1989; Olea, 1991). Therefore, seeking suitable variogram model to provide prior covariance matrix reasonably is the key of Kriging interpolating for some kind space data.

In fact, variograms are so important to Kriging that several authors have discussed different methods for variogram experimentation and fitting from a range of perspectives (David, 1977; Journel and Huijbregts, 1978; Cressie and Hawkins, 1980; Omre, 1984; Armstrong, 1984; Journel, 1987, 1988; Isaaks and Srivastava, 1988, 1989; Cressie, 1993; Deutsch and Journel, 1998). One general point in these discussions is that a variogram is a function of the distance and direction or of only the distance, i.e., when defining an azimuth-based variogram. This is why Kriging is referred to as spatial statistics. The exact method of experimenting with or fitting a variogram depends on the distribution of the spatial data. However, in general, the spatial data distribution assumes that the spatial variation is a function of the distance and direction; therefore, nearly all variograms structured so far are defined by distance–direction or using other orientations-related method, such as polar coordinates (Iwashita et al., 2005).

Because the evaluation of cobalt-rich crusts on seamounts requires spatial interpolation, the Kriging method needs to deal with a type of spatial data that has not previously drawn attention. We tried to apply conventional Kriging to the evaluation of

* Corresponding author at: First Institute of Oceanography, State Oceanic Administration, Qingdao 266061, China.
E-mail address: dwendu@fio.org.cn (D. Du).

http://dx.doi.org/10.1016/j.oregeorev.2016.12.028
0169-1368/

cobalt-rich crust resources on seamounts; however, the variogram could not suitably describe the self-correlation of the cobalt-rich crusts. This may be the reason why there are no reports of mineral resource estimations or reserve calculations based on Kriging for seamounts. Spatial data zonation is generally thought to account for the spatial geometric anisotropy of variograms (Isaaks and Srivastava, 1989; Goovaerts, 2012). Mineral resources on land, which are subjected to strata or linear structures such as faults, are usually zonal in distribution. Their variograms are spatially anisotropic and are a function of the azimuthal direction. On seamount surfaces, the spatial distribution of mineral resources is different and is subjected to water depth and slope gradients around the seamount, and consequently, their anisotropy appears to have a circular or radial distribution. Therefore, the application of an azimuth-based variogram algorithm to seamount surface data is irrational. In this study, we proposed a new variogram model for the unique spatial data of a seamount surface, through which Kriging can be successfully applied to estimate the spatial thickness distribution of cobalt-rich crusts on a seamount surface.

These data are referred to here as three-dimensional (3D) surface random variables, and they will be discussed in more detail in the next section.

2. Conventional variograms are invalid for cobalt-rich crust deposits

2.1. Distribution features of cobalt-rich crusts on seamounts

A seamount is a submarine volcanogenic conical or flat-topped (guyot) mountain rising hundreds to thousands of meters above the seafloor or even above the sea level as islands. Cobalt-rich crusts occur on the sediment-free surfaces of seamount slopes and the summit and have attracted economic interest owing to the potential for manganese, cobalt, nickel, rare earth elements, tellurium, and platinum resources (Hein et al., 1999; Hein, 2000). Therefore, explorations and eventual resource evaluations are being conducted.

Cobalt-rich crusts occur on seamounts at water depths between 400 and 7000 m; however, the most promising cobalt-rich crusts, as determined from exploration, are at water depths less than 2500 m. Crusts shallower than 2500 m are thick and show high grades of cobalt, nickel, and other metals relative to those at deeper water depths (Usui and Someya, 1997; Hein, 2000; Zhang et al., 2008). The survey stations in this study for cobalt-rich crust exploration are located within the 1500–4000 m interval.

Since the 1990s, the Magellan Seamounts located in the western part of the Pacific (as shown in Fig. 1) have been investigated as promising objects for cobalt-rich crust deposits by geologists from the China Ocean Mineral Resources R&D Association (COMRA). The main purpose of this paper is to present a Kriging method to estimate the distribution of cobalt-rich crusts on a guyot. Here, we chose the ME guyot as an experimental field to test our method; its location is shown in Fig. 1. The bathymetric data for the guyot were obtained by a Simrad EM120 multibeam echo sounder, and thickness data of the cobalt-rich crusts were derived from geological sampling (submarine drilling and dredging).

The area shallower than 1500 m on the ME guyot is the flat summit, which is covered by sediments, and no exposed cobalt-rich crusts are found there. The area between 1500 and 4000 m is the slope of the seamount, which is covered by cobalt-rich crusts. The crust survey stations are located on the slopes, where the gradient varies from 5° to 40°. During exploration, the parameters used for the resource estimates were obtained via sampling (primarily submarine drilling) at these stations, and the data obtained included thickness, abundance (weight of the wet crust per unit area) of the seabed, and element concentrations of the

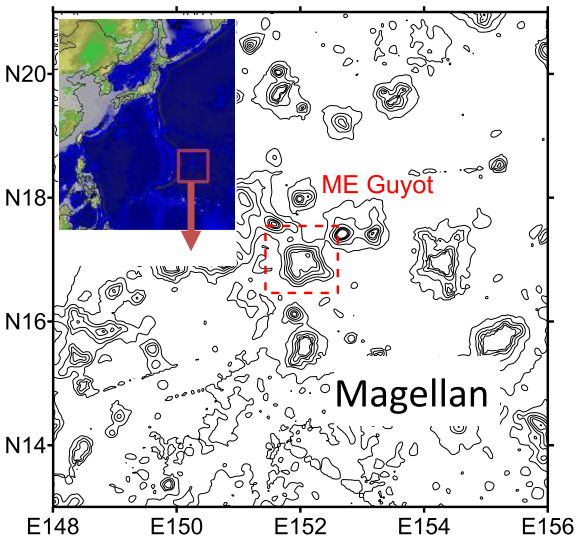

Fig. 1. Location of the Magellan Seamounts and the ME guyot.

cobalt-rich crusts. The crust thickness, a critical parameter for resource estimates, was selected as the experimental data. Studies have demonstrated that the crust distribution is generally subjected to rock outcrop distributions and slope gradients, rather than to linear structures oriented in a certain direction, which usually control the distribution of ore bodies on land. In other words, we cannot use a distance–direction-defined variogram to express the spatial self-correlation and anisotropy of cobalt-rich crusts on seamount surfaces.

2.2. The inapplicability of conventional variograms

We first tested the viability of a conventional variogram theory to estimate the thickness of the cobalt-rich crusts using the distance–direction-based pairs search principle (Deutsch and Journel, 1998).

As shown in Fig. 2, the stations on the cobalt-rich crusts are distributed along a closed slope annuli. We assumed that E–W is 0°, NE–SW is 45°, S–N is 90°, and NW–SE is 135°. According to the pairs search principle of conventional variogram algorithms, at points A or D, the 0° pairs fall on the contour line, and the 90° pairs

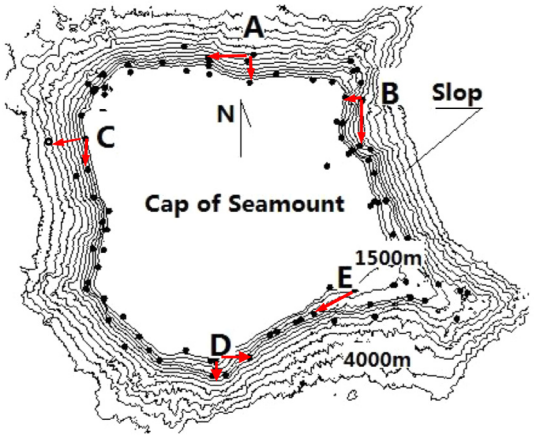

Fig. 2. Topography of the ME guyot with several survey stations indicated for cobalt-rich crusts (the red arrows indicate that these point pairs form head-to-end-point searching pairs). (For interpretation of the references to colour in this figure legend, the reader is referred to the web version of this article.)

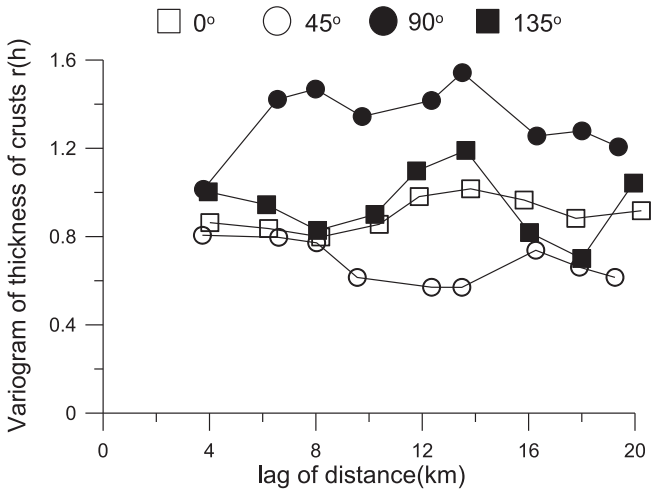

Fig. 3. The distance–direction-based experimental variogram.

are in the maximum gradient direction. Conversely, at points B or C, the 0° pairs are in the maximum gradient direction, whereas the 90° pairs fall on the contour line. At point E, the relative azimuth of the pairs on the contour line is 30° (or 210°). This suggests that, given that the spatial data distribution of the seamount surface is subjected to water depth and slope gradients, the distance–direction-based pairs search principle is inconsistent with the spatial data distribution. That is, an experimental variogram using distance–direction-based pairs search does not reflect the self-correlation and anisotropy of the spatial data on the seamount surface. This observation is also confirmed by the variogram calculated on the basis of distance–direction.

Fig. 3 shows the scatter points of the experimental variograms in the 0°, 45°, 90°, and 135° directions calculated with the GAVM3.FOR program of the GSLIB package using the calculation algorithm for experimental variograms described by Deutsch and Journel (1998). The sill values of these variograms vary greatly from one direction to another, ranging from 0.7 in the 45° direction to 1.4 in the 90° direction. In each direction, the variation is independent of the distance, which means that it does not vary with distance. The resulting variogram does not reflect the self-correlation of the spatial data. Having shown that the distance–direction-based pairs search is not valid, we considered a search based on distance alone. However, if direction is not included, we must assume that the mineral resources on the seamount slopes are spatially isotropic, which is not consistent with the exploration data. This further indicates that Kriging with conventional variograms is not effective in estimating mineral resources on seamounts and could explain why Kriging has not previously been effectively applied to estimate mineral resources on seamounts.

On the basis of the spatial distribution features of cobalt-rich crust resources on seamount surfaces, we propose the designation of a generalized 3D surface variable and provide a new distance–gradient-based variogram experimentation and fitting algorithm to apply Kriging in estimating mineral resources on seamounts.

3. 3D surface random variables

In general, Z is used to represent a random variable and a function of the coordinates. Expressed as $Z(x, y, v)$, it is a vector function in a typical 3D coordinate system, as shown in Fig. 4. For example, this random variable can represent the salinity in a 3D ocean domain φ because the determined salinity exists at any point in the defined domain φ. Such a typically defined domain or random

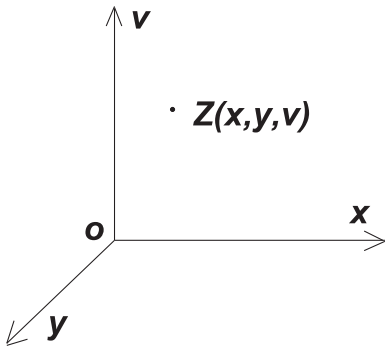

Fig. 4. A random variable Z in the 3D system.

field of 3D variables has not only a length and width but also a thickness. In other words, they can be continuously evaluated in the x, y, and v directions. If only the sea surface salinity data are included, this can be expressed by $Z(x, y)$. If the former is called a 3D random variable, then the latter can be called a 2D random variable. These two types of spatial data are the 3D and 2D spatial variables dealt with by the GSLIB package.

If cobalt-rich crust parameters on a seamount slope surface are taken to be random variables, are they 3D or 2D random variables? When estimating space variables, some studies treat the water depth as the vertical coordinate and decide that it is a 3D random variable (Soleimani et al., 2008; Bonté et al., 2010), whereas other studies ignore the water depth and treat it as a 2D random variable defined by geographic coordinates (Nwankwoala et al., 2012). In our opinion, it is technically neither a 3D nor a 2D random variable but rather a 3D surface random variable that can be expressed as $Z(x, y, dp)$. In variogram experimentation, $Z(x, y, dp)$ represents the thickness data of cobalt-rich crusts on a slope at the geographic position (x, y) and the water depth dp, as shown in Fig. 5.

In addition to the general characteristics of an ordinary random variable, a 3D surface random variable in this study has the following characteristics.

(1) The defined domain φ is a curved surface of a 3D space (Fig. 5).

$$Z(x, y, dp) \in [\varphi : (x_{\min} \leqslant x \leqslant x_{\max}, y_{\min} \leqslant y \leqslant y_{\max}, dp_{\min} dp \leqslant dp_{\max})]$$

(2) When (x, y) is determined, dp is a unique value that coincides with (x, y).

(3) The expected random variable $Z(x, y, dp)$ does not vary with position; its spatial variation is decided by both distance and relative water depth, Δdp, or gradient, g, but is independent of direction.

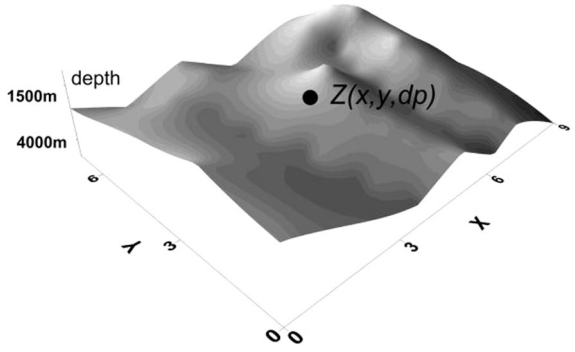

Fig. 5. A random variable Z on the 3D surface.

Because the 3D surface random variable in this study is neither a 3D nor a 2D random variable, conventional variogram experimentation and fitting algorithms are not applicable when calculating its variogram.

4. Distance–gradient-based variogram

4.1. Experimental variogram

Owing to the assumption of the stationarity of a random variable in GSLIB, we assume that (a) the expectation of a 3D surface random variable does not vary with the exact position and (b) the variance of the random variable exists and does not depend on direction but rather on the spatial distance and relative water depth (or gradient).

A variogram is conventionally defined as half of the arithmetic mean of the variance of data pairs defined by the distance–direction vector h (Fig. 6a), which can be expressed by Eq. (1). Correspondingly, the variogram of a 3D surface random variable is defined as half the arithmetic mean of the variance of data pairs defined by the distance–gradient, which can be expressed by Eq. (2). These types of data pairs are shown in Fig. 6b. If the relationship between these data pairs is described by a right-angle triangle and the distance ds is determined, one more parameter, either the water depth dp or gradient g, is sufficient to define a certain right-angle triangle, and eventually, the spatial relationship between the data pairs can be determined. Because dp and g are equivalent in our definition, we chose to experiment with g in this study and fit the variogram based on the distance–gradient (ds–g).

$$r(h) = \frac{1}{2N(h)} \times \sum_{i=1,\dots,n\, j=1,\dots,n}^{N(h)} [z(x_i, y_i, v_i) - z(x_j, y_j, v_j)]^2 \quad (1)$$

$$r(ds, g) = \frac{1}{2N(ds, g)} \times \sum_{i=1,\dots,n\, j=1,\dots,n}^{N(ds,g)} [z(x_i, y_i, dp_i) - z(x_j, y_j, dp_j)]^2 \quad (2)$$

Assume that there are n data points, $z(x_i, y_i, dp_i), i = 1, \dots, n$. When the head point $z(x_h, y_h, dp_h)$ is determined, the end point $z(x_t, y_t, dp_t)$ is searched at a certain distance and in a certain gradient following the steps below.

4.1.1. Calculating the distance and gradient of data pairs

$$\text{Spatial distance}: ds'_{ht} = squrt\left[(x_h - x_t)^2 + (y_h - y_t)^2 + (dp_h - dp_t)^2\right]$$

$$\text{Horizontal distance}: ds_{ht} = squrt\left[(x_h - x_t)^2 + (y_h - y_t)^2\right] \quad (3)$$

Because the horizontal distance is involved in the calculation of the gradient, the horizontal distance is used in this study as a distance-measuring parameter instead of the spatial distance. Therefore, in this paper, distance hereafter refers to horizontal distances.

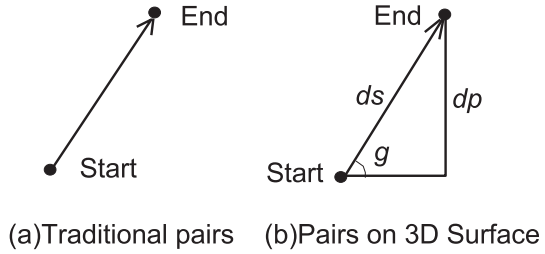

Fig. 6. Data pairs in an experimental semi-variogram.

The gradient is defined as

$$g_{ht} = \begin{cases} \arctan\left[\frac{dp_h - dp_t}{ds_{ht}}\right] \times \frac{180.0}{\pi} & , ds_{ht} \neq 0.0 \\ 0.0 & , ds_{ht} = 0.0 \end{cases} \quad (4)$$

4.1.2. Statistical distribution and grouping of gradients

Given that there are n experimental points, there are a total of $\frac{n^2}{2}$ gradient data. The maximum gradient is $g_{\max}$, and the minimum is $g_{\min}$. Gradients are divided into three equal-frequency groups: the high-gradient group (gradient 3), middle-gradient group (gradient 2), and low-gradient group (gradient 1). The boundary gradient between the high- and middle-gradient groups is g_{big}, and that between the low- and middle-gradient groups is g_{small}. Three gradient groups of data pairs submit to following formula, and as illustrated in Fig. 7

$$\begin{cases} gradient\ 3 : g_{big} \leqslant g \leqslant g_{\max} \\ gradient\ 2 : g_{small} \leqslant g \leqslant g_{big} \\ gradient\ 1 : g_{\min} \leqslant g \leqslant g_{small} \end{cases} \quad (5)$$

4.1.3. Search distance

The distance search follows the principle described by Deutsch and Journel (1998). Pairs within a specific lag distance are searched according to the lag distance and the lag tolerance. The eventual statistical lag distance is the mean of each group.

4.1.4. Calculating the experimental variogram

For a certain distance ds and gradient g, $N(ds, dp)$ pairs are obtained, and the variogram is calculated from Eq. (2). The corresponding distance ds and gradient g are the mean distance and mean gradient of the group. Consequently, the distance-variogram data of the three gradient groups can be derived.

4.1.5. Experimental variogram diagrams

Fig. 8 shows the distance–gradient-based variogram diagram of the thickness of the cobalt-rich crusts on the ME guyot. First, distance-variation scatter diagrams are produced (Fig. 8). Then, the variogram is preliminarily fitted with artificial curves. Finally, the mean square deviation c, nugget c_0, and range a are estimated according to the variogram curve, where gradient g is the mean gradient.

The variogram shown in Fig. 8 is grouped according to gradient instead of direction. The mean gradients of the three groups are

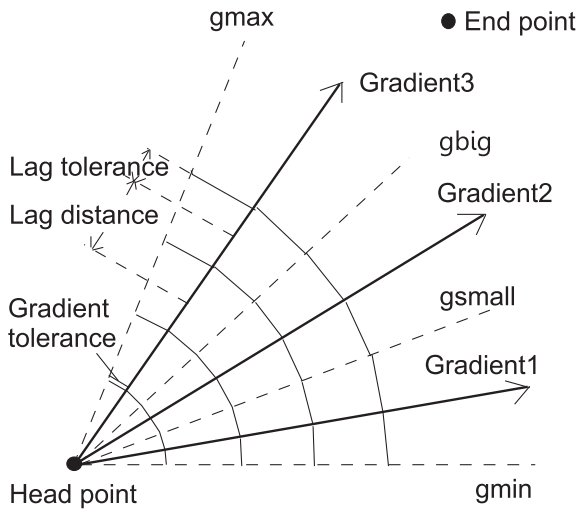

Fig. 7. Formulae for pairs look for one another based on the distance and gradient.

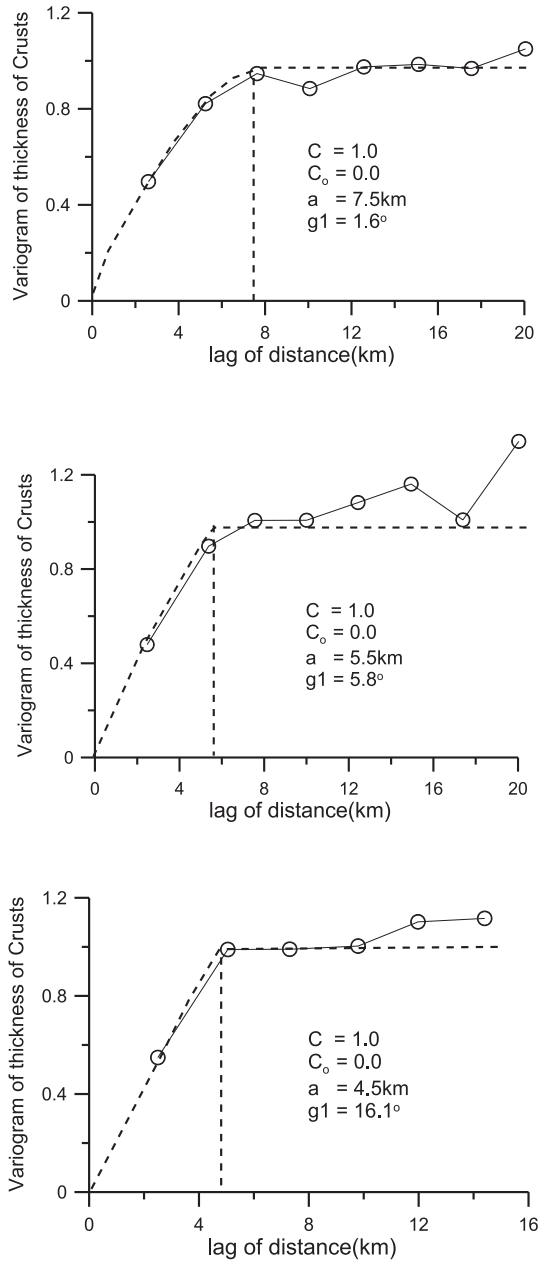

Fig. 8. Distance–gradient-based experimental variogram.

1.6°, 5.8°, and 16.1°, respectively, and the corresponding ranges are 7.5, 5.5, and 4.5 km, respectively. The sill is close to 1.0, and the nugget c_0 is 0.0 for all three groups. Comparisons with the distance–direction-based experimental variogram (Fig. 3) indicate that the distance–gradient-based variogram algorithm is more suitable for mineral resource data on the slopes of seamounts.

4.2. Theoretical variogram

4.2.1. Range–gradient function

Only when a range is fitted to a continuous gradient function can it support the fitting of any theoretical variogram and be applied to Kriging. Gendzwill and Stauffer (1981) and Deutsch and Journel (1998) attempted to fit the anisotropy of ranges with spheroidal functions in polar coordinates. However, we attempt to fit the gradient–range function with the Cartesian coordinate system and plot the three groups of gradients and ranges (1.6, 7.5), (5.8, 5.5), and (16.1, 4.5) of the experimental variogram into the gradient–range Cartesian coordinate system (Fig. 9), in which the range is virtually inversely proportional to the gradient.

The inverse relationship between the range and gradient indicates that it is reasonable to use a reciprocal function $a = \frac{1}{g}$. The extended reciprocal function shown in Eq. (6) was used in this study to fit the range–gradient function.

$$a = a_0 + \frac{p}{g+1} \tag{6}$$

where a is a range function with gradient g as an independent self-variable and a_0 and p are the undetermined constants. When gradient $g = 0$, the range is $a_0 + p$, and when the gradient is very large, the range is close to a_0. The two undetermined constants a_0 and p in Eq. (6) can be solved when two data points on the curve are known. Now, we substitute data from the gradient 3 and gradient 1 groups $(g_3, a_3), (g_1, a_1)$, respectively, into Eq. (7) to derive the undetermined

$$\text{constants } a_0 \text{ and P}: \begin{cases} p = \frac{a_1 - a_3}{\frac{1}{g_1+1} - \frac{1}{g_3+1}} \\ a_0 = a_1 - \frac{p}{g_1+1} \end{cases} \tag{7}$$

and then substitute Eq. (7) into Eq. (6) to derive the fitted range–gradient function.

To test the fitness of fitting using this function, we can substitute data from the gradient 2 group, (g_2, a_2), into Eqs. (6) and (7) to derive the theoretical range of this group, a_2^*, and then compare the relative error between a_2^* and a_2 to see how well the range–gradient function is fitted. We could also put this group of data (g_2, a_2) into the Cartesian coordinate system in Eq. (6) as shown in Fig. 9 to test whether (g_2, a_2) falls onto the simulated range–gradient curve and, therefore, how well the range–gradient function is fitted.

For the thickness data of cobalt-rich crusts on the experimental seamount, we substituted data from the gradient 3 and gradient 1 groups, (1.6, 7.5) and (16.1, 4.5), respectively, into Eq. (6) and got $a_0 = 4.0$ and $p = 9.2$. The fitted range–gradient function is therefore

$$a(g) = 4.0 + \frac{9.2}{g+1} \tag{8}$$

The curve of Eq. (8) is shown in Fig. 9. Then, using the range–gradient data of the gradient 2 group (5.5, 5.8) as the inspection point for the function fitting, we substituted gradient 5.8 into Eq. (8) and derived the theoretical range of 5.4, which is only 0.1

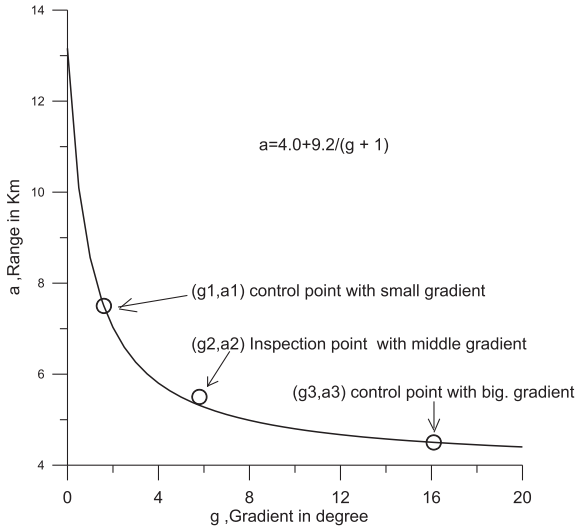

Fig. 9. The three experimental points (g, a) and the gradient–range fitted function.

lower than the experimental range with a relative error of 1.8%. When we plot (5.5, 5.8) into the range–gradient Cartesian coordinate system, this point falls very close to the theoretical curve. This testing result indicates that this is a satisfactory fitting function.

4.2.2. Theoretical variogram fitting

The range–gradient extended reciprocal function obtained by fitting was substituted into the theoretical variogram model, which, as proposed by Deutsch and Journel (1998), can be a spherical model, an exponential model, or a Gauss model. For this demonstration, we used the spherical model function.

$$r(ds,g) = c \times Sph\left(\frac{ds}{a}\right) = \begin{cases} c \times \left[1.5 \times \frac{ds}{a} - 0.5 \times \left(\frac{ds}{a}\right)^3\right] & ,if\ ds \leqslant a \\ c & ,if\ ds > a \end{cases} \quad (9)$$

We substituted Eq. (6) into Eq. (9) and derived the theoretical distance–gradient variogram as shown in Eq. (10).

$$r(ds,g) = c \times Sph\left(\frac{ds}{a}\right) = \begin{cases} c \times \left[1.5 \times \frac{ds}{a_0 + \frac{p}{g+1}} - 0.5 \times \left(\frac{ds}{a_0 + \frac{p}{g+1}}\right)^3\right] & ,if\ ds \leqslant a_0 + \frac{p}{g+1} \\ c & ,if\ ds > a_0 + \frac{p}{g+1} \end{cases} \quad (10)$$

Eq. (10) does not include the nugget effect. a_0 and p are undetermined constants derived by fitting the range of the experimental variogram. If the nugget effect is included, then Eq. (10) is transformed into Eq. (11):

$$r(ds,g) = c_0 + (c - c_0) \times Sph\left(\frac{ds}{a}\right) \quad (11)$$

It may also be transformed into a covariogram:

$$\mathrm{cov}(ds,g) = (c - c_0) \times \left[1 - Sph\left(\frac{ds}{a}\right)\right] \quad (12)$$

In our example, $a_0 = 4.0$, $p = 9.2$, and c is the sill value or variance contribution. The calculated experimental variogram of the seamount test data in our study is 1.0. The fitted variogram in Eq. (10) is shown in Fig. 10.

The most prominent features of this theoretical variogram are that it is subjected to the gradient rather than the direction, as are conventional generalized variables, and that the variogram is a function of the distance and gradient.

4.2.3. Concerning positive definiteness

It is time-consuming and difficult to test the positive definiteness of a particular variogram model (Armstrong and Jabin, 1981), even though a method for testing variograms for positive definiteness was given by Armstrong and Diamond (1984). This is one of the reasons why we adopted conventional and reliable spherical functions to fit the variogram or covariogram. After all, spherical functions, Eqs. (11) or (12), were used ultimately in the Kriging equations and insured that the variograms had positive definiteness, as in other applications.

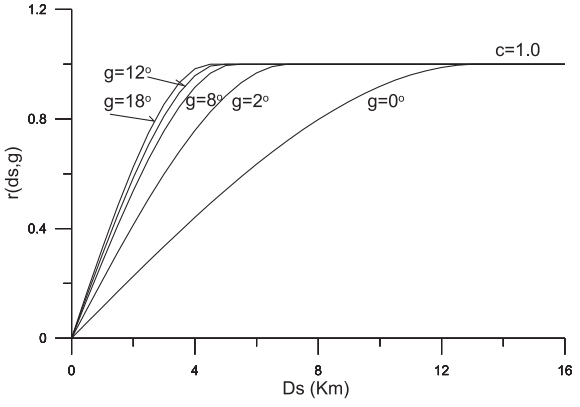

Fig. 10. Variogram modeling for different gradients.

4.3. Procedure

4.3.1. Test for data stationarity

The stationarity parameter of random variables is tested using a normal distribution or lognormal distribution hypothesis method. If the data in the study area are confirmed to have a normal distribution, then they are regarded as approximate random stationary generalized variables and can be processed with experimental variogram calculations and Kriging estimations.

4.3.2. Gradient statistics

Eq. (4) was used to calculate the relative topographic gradient between the regional grid nodes in the area to be estimated by Kriging, as well as the gradient between the station pairs, to extract the maximum gradient, minimum gradient, mean gradient, and standard error of the gradient required for gradient grouping. Water depth data were generally high-accuracy water depth data acquired by a multibeam sonar sounding system.

4.3.3. Gradient grouping of the experimental variogram

On the basis of Eq. (5) and with reference to the statistical information in the topographic gradients, the stations were grouped according to the three gradient groups.

The low-gradient group (gradient 1) represents the search orientation of the approximate contour. The middle-gradient group (gradient 2) represents the search orientation of the transitional gradient between the fathom line and the maximum gradient. The high-gradient group (gradient 3) represents the search orientation of the approximate topographic gradient. The ranges and gradients of the gradient 1 and gradient 3 groups were involved in the fitting of the range–gradient function, and those of the gradient 2 group were used as test data for the fitting effect to verify the validity of the fitting of the range–gradient function.

4.3.4. Pilot calculation of the experimental variogram

The experimental variograms of each of the three gradient groups were calculated using the method described in Section 4.1 by adjusting the parameters, lag distance, lag tolerance, gradient, and gradient range multiple times.

4.3.5. Gradient–range function fitting

Using the method described in Section 4.2, the gradient–range function was fitted with the experimental gradient and range data of the gradient 1 and gradient 3 groups. Then, the resulting gradient–range function was tested with the experimental range and gradient data from the gradient 2 group. If the result is not satisfactory, the extended reciprocal function, Eq. (6), can be adjusted by replacing $(g + 1)$ with $(g + 1)^n$, where n can be 1/3, 1/2, 1, 2 or 3. In our experiment, $n = 1$. Note that there may be other fitting functions that could provide a better fitting that has not yet been determined.

4.3.6. Variogram fitting

This is a process that substitutes the gradient–range function into a spherical model function, an exponential model function, or any other model function as appropriate, as described in detail in Section 4.2.

4.3.7. Testing the variogram fitting effect

The fitting effect of a variogram includes the fitness between the fitting curve and the test points and the Kriging effect. If the effect is not satisfied, then return to 4.3.3.

5. The FORTRAN program

5.1. The experimental variogram program

Using the method described in Section 4.1, the variogram program GAMV.for in the GSLIB package and its GAMV.INC were modified. The resulting program and its notes are shown in the program's source code. To distinguish it from the original, we renamed the modified program GAMV-3dsurface.for, as detailed in Appendix 1. To respect the contribution of the original program, the modified program was only used for the distance–gradient-based calculation of the experimental variograms.

5.2. Fitting of the variograms and generation of the covariance matrix

Using the method described in Section 4.2, KB2D.for in the GSLIB package and its KB2D.INC were modified by rewriting the subprogram of the covariance matrix and adding an extracted function module of the water depth. The resulting program and its notes are shown in the program's source code. To distinguish it from the original, we renamed the modified program kb-3dsurface.for, as detailed in Appendix 2. To respect the contribution of the original program, the modified program was only used for the distance–gradient-based Kriging calculation of the variograms.

5.3. Runtime program environment

The computer system environment for the program modification and runtime were the Windows 7 system and the Visual Fortran 6.0 compiler, respectively.

6. Estimating the distribution of cobalt-rich crust thicknesses on the ME guyot

6.1. Data preparation

6.1.1. Coordinate transformation

The data (lonx, laty) represent the longitude and latitude, which are transformed into the plane coordinates (x, y). First, the origin of the coordinate system was selected, which can be the minimum longitude and latitude of the study area (lat0, lon0). Then, it was approximately transformed using the following formula:

$$\begin{cases} x = (lonx - lon0) \times 1.852 \times 60.0 \times \cos(laty) \\ y = (laty - lat0) \times 1.852 \times 60.0 \end{cases}$$

For a more accurate transformation of the coordinates, please refer to literature related to coordinate transformations (Dutch, 2005).

6.1.2. Information point data

The information point data are the spatial data to be processed. For the purpose of our study, the experimental data are the thickness data of the cobalt-rich crusts on the surface of the seamount, which are saved in a text file called Seamounts.TXT. This file uses the same format as cluster.dat in the GSLIB package, the x-axis in km is in column 1, the y-axis in km is in column 2, the water depth in m is in column 3, and the crust thickness in mm is in column 4.

6.1.3. Data stationarity test

The stationarity of the data is tested in the conventional way. If the data show a normal distribution, they are considered to be approximately stationary and can be processed with variogram experimentation and fitting. If they do not, they may be partially smoothed as appropriate, or a proper minimum and maximum distinguished value interval may be specified to remove the outliers. This feature is performed by the variable limits in line 6 of the parameter file.

Fig. 11 shows a histogram of the experimental data. As tested by the normal distribution hypothesis method, the histogram shows a normal distribution, and the experimental data are therefore considered to be of a weakly stationary random variable.

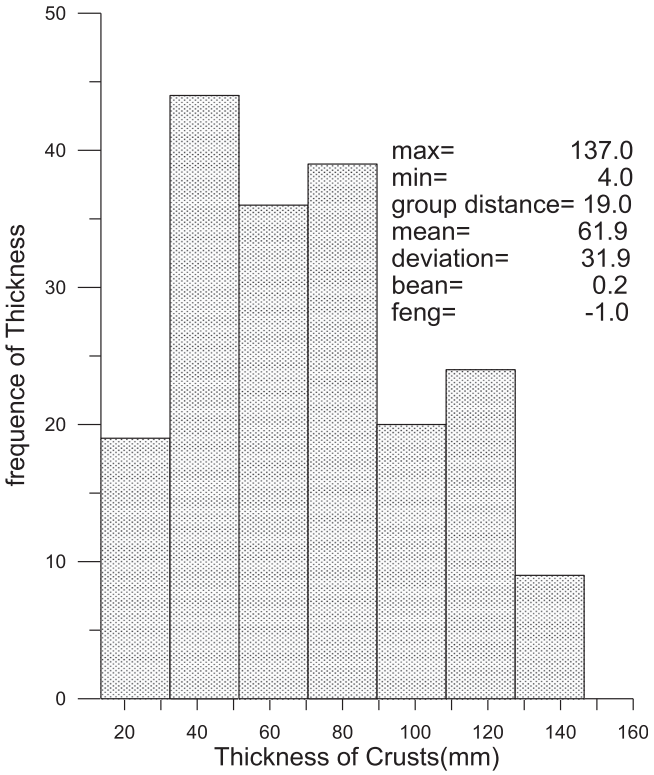

Fig. 11. Statistical histogram of the thickness of the crust on a seamount.

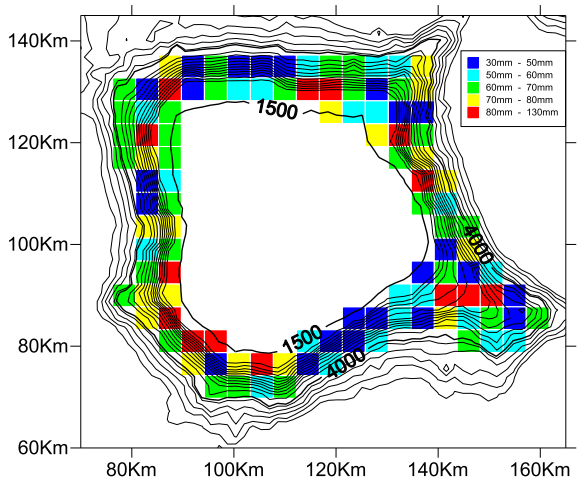

Fig. 12. Distribution thicknesses of the cobalt-rich crusts estimated using Kriging with the distance–gradient-based variogram.

6.1.4. Determining the effective water depth interval

The distribution of cobalt-rich crust resources on seamounts primarily depends on the stratified structure of the seawater and the hydro-chemical characteristics. These cobalt-rich crusts are generally found on seamount flanks and summits at 800–4000 m water depth; however, this can vary between seamounts. The minimum water depth is generally the platform depth of a guyot or the minimum water depth of a conical seamount; the maximum water depth is the baseline for the surrounding abyssal sediment plain. However, the likely maximum water depth for mining a guyot will be approximately 2500 m, and rugged conical seamounts will not be mined (Hein et al., 2009). The effective water depth interval is defined by the maximum water depth *dpmax* (or $dp_{\max}$) and the minimum water depth *dpmin* (or $dp_{\min}$) and is determined by modifying line 7 of gavm.par and line 6 of Kb-3Dsurface.par.

6.1.5. Water depth data

The data we processed are those relating to seamount mineral resources. Variable $Z(x, y, dp)$ is a function of the geographic coordinate (x, y) and the water depth dp. Water depth data are indispensable; they appear not only at the existing data points but also at any position over the entire estimated area.

The water depth data used here were acquired by a multibeam sonar sounding system and are 100 m × 100 m grid data. The data are saved in the text file ME.DAT. This data file appears in line 7 of the parameter file Kb-3Dsurface.par.

For the purpose of Kriging estimation, a geographic coordinate can be taken anywhere; however, not all points provide water depth data. In such cases, we can use interpolation to generate the water depth data at any point from the ME.DAT file data. In our study, a simple interpolation function was used to derive the

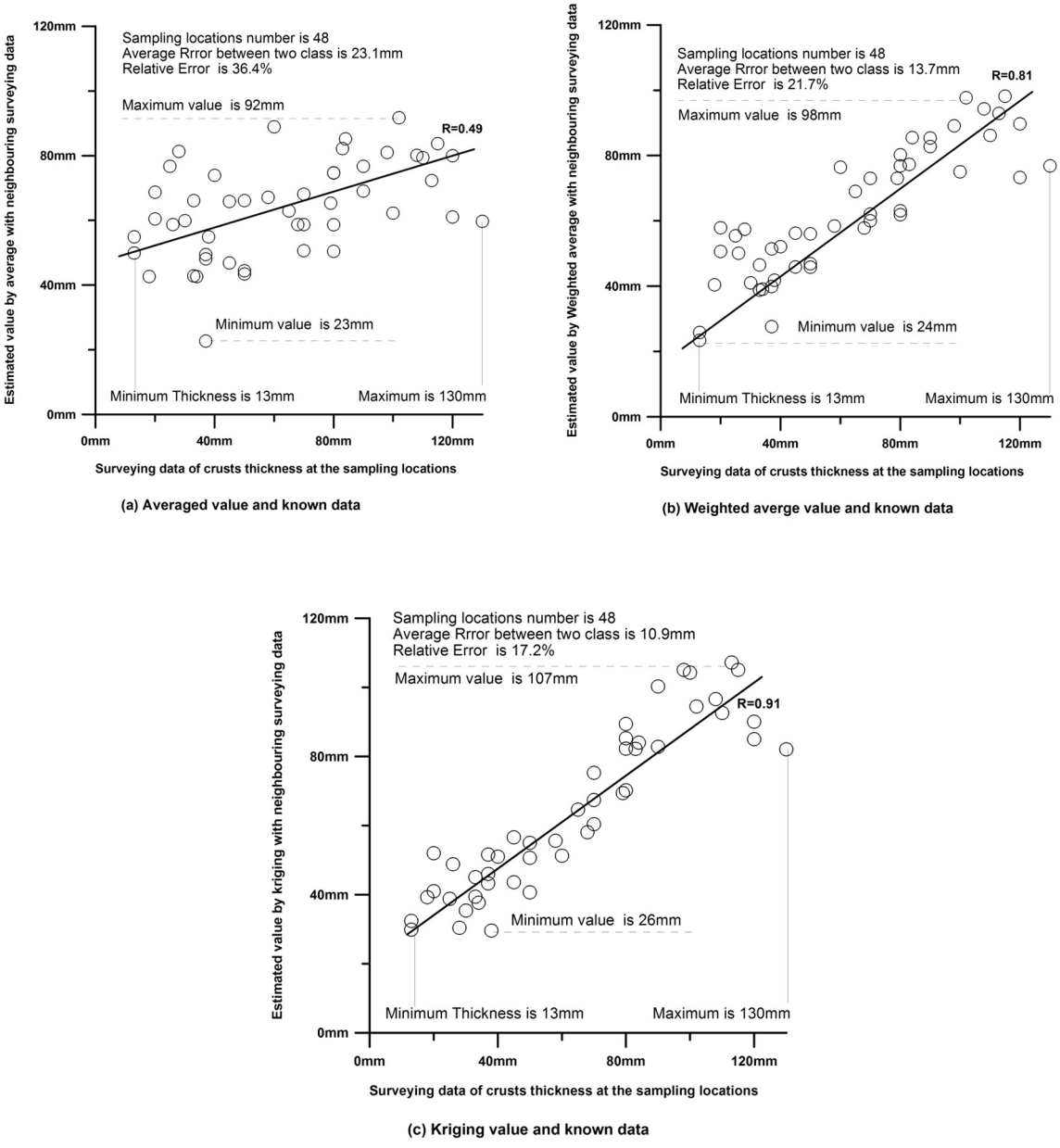

Fig. 13. Scatter plots with the surveying data and its estimated values of the crust thicknesses in the *x* and *y* coordinates, respectively. The 48 locations with surveying data of the crust thickness were estimated using three different methods. The point interpolation search radius was 10 km, the maximum number of data points was 9, and the minimum number of data points was 3. Average error = ∑abs(surveying data − estimated value)/48. Relative Error = 100 * Average error/mean of 48 surveying data (%).

water depth data. This simple function, get_depth(x,y), is included in the file 3DSurface.for.

6.2. Estimated value of the cobalt-rich crust thicknesses

The Kriging estimation was performed on a 3 × 3 block in units of 4472 m × 4472 m square with a horizontal area of 20 km^2, equivalent to the minimum grid unit area required by the Regulations on Prospecting and Exploration for Cobalt-rich Crusts issued by the International Seabed Authority. With the estimation results, the resource area was mapped according to the agreement of the International Seabed Authority. The thickness values of the cobalt-rich crusts for the 108 grid cells (4472 m × 4472 m) estimated by the modified Kriging method in this paper are shown in Fig. 12.

6.3. Performance evaluation

Quantitatively evaluating how well the interpolation actually predicts known values using subsets of the surveying data could demonstrate that the distance–gradient-based variogram and Kriging have improved the interpolation method for estimating cobalt-rich crust thicknesses on seamounts. The forecasting effects for the method in this paper, the average method, and the inverse distance weighting (Lu and Wong, 2008) method were used for interpolations. These three methods were set using the same interpolation parameters, i.e., the same search radius and the same point number of data points. The value of a point that was estimated is not used in the calculation; however, several neighboring known data points participate in the calculation as information points. Therefore, each of the 48 locations (subsets of the surveying data) has two sets of values for the cobalt-rich crust thickness: a set of known data obtained by surveying and a set of forecasted values estimated by the spatial interpolation method.The two sets of values were projected into the 2D coordinate system, and three scatter plots of the known data and the estimated values were generated corresponding to the three interpolation methods, as shown in Fig. 13a–c, respectively. The average error and relative error, the correlation coefficient between the two sets of values, and the maximum and minimum values are marked in the figure. The forecasting effects of three methods are obviously different. Of the three, the distance–gradient-based variogram Kriging (here referred to as the Kriging) has the smallest average and relative errors and the largest correlation coefficient. In all three methods, the maximums and minimums of the estimated values approached the means; this reflects the smoothing effect of interpolations. The smoothing effect of the Kriging method was smaller than that of the other methods. In this case, the Kriging method is obviously superior.

Surveying samples are expensive, and location data on seamounts are sparse; therefore, the interpolation method used is particularly important. A good interpolation effect indicates the considerable prospects of applying this method.

7. Conclusions

The distribution of mineral resources on seamount slopes is subjected to water depth and gradients and does not display spatial zonation like land deposits, which are subjected to linear structures. The conventional distance–direction-based variogram algorithm is not valid for mineral resource valuation of cobalt-rich crusts on seamounts. However, the distance–gradient-based variogram algorithm presented here was demonstrated to be effective and could derive better results than the average method or the inverse-distance weighting method.

Note that many guyots, including those under exploration contracts, are not capped by sediment, and cobalt-rich crusts do occur on their summits. Because the summits of guyots are not really flat but consist of stepped terraces, furrows, and low-relief ridges among other topographic features, the procedures developed here will be applicable to these guyots as well. In addition, other values can be estimated using this technique, for example, cobalt concentrations can substitute for crust thickness in these calculations.

Improvements in this variogram algorithm might result in the application of Kriging to mineral resource evaluations or reserve estimations for cobalt-rich crusts on seamounts. The ranges and corresponding different slope gradients could provide references for the design of sampling sites when surveying the seamounts; in addition, they suggest that the spacing of the sampling sites should be smaller than the ranges.

Acknowledgements

Funding was provided by the China Ocean Mineral Resources R&D Association (Programs: DY125-13-R-03 and 06) and by the National Nature Science Foundation of China (Program: No. 41306059).

Appendix A. Supplementary data

Supplementary data associated with this article can be found, in the online version, at http://dx.doi.org/10.1016/j.oregeorev.2016.12.028.

References

Armstrong, M., 1984. Improving the estimation and modelling of the variogram. In: Geostatistics for Natural Resources Characterization. Springer, Netherlands, pp. 1–19.
Armstrong, M., Diamond, P., 1984. Testing variograms for positive-definiteness. Math. Geol. 16 (4), 407–421.
Armstrong, M., Jabin, R., 1981. Variogram models must be positive definite. Math. Geol. 13 (5), 455–459.
Bonté, D., Guillou-Frottier, L., Garibaldi, C., Bourgine, B., Lopez, S., 2010. Subsurface temperature maps in French sedimentary basins: new data compilation and interpolation. Bull. Soc. géol. Fr. 181 (4), 377–390.
Cressie, N.A., 1993. Statistics for Spatial Data. Wiley, New York.
Cressie, N., Hawkins, D.M., 1980. Robust estimation of the variogram: I. J. Int. Assoc. Math. Geol. 12 (2), 115–125.
David, M., 1977. Geostatistical ore reserve estimation. In: David, M. (Ed.), Developments in Geomathematics. Elsevier, Amsterdam, p. 364.
Deutsch, C.V., Journel, A.G., 1998. GSLIB geostatistical software library and user's guide. Oxford University Press, New York, pp. 20–100.
Dutch, S., 2005. Converting UTM to Latitude and Longitude. <http://www.uwgb.edu/dutchs/UsefulData/UTMFormulas.htm>.
Gel'fand, I.M., Jakubski, Z., 1961. Generalized Random Processes. Trw, Space Technology Labs Los Angeles Calif.
Gendzwill, D.J., Stauffer, M.R., 1981. Analysis of triaxial ellipsoids: their shapes, plane sections, and plane projections. J. Int. Assoc. Math. Geol. 13 (2), 135–152.
Goovaerts, P., 2012. Geostatistics for natural resources evaluation. J. Environ. Qual. 42 (4), 437–438.
Hein, J.R., 2000. Cobalt-rich ferromanganese crusts: global distribution, composition, origin and research activities. In: Proceedings of International Seabed Authority workshop minerals other than polymetallic nodules of the international seabed area, 26–30.
Hein, J.R., Conrad, T.A., Dunham, R.E., 2009. Seamount characteristics and mine-site model applied to exploration and mining-lease-block selection for cobalt-rich ferromanganese crusts. Marine Georesour. Geotechnol. 27 (2), 160–176.
Hein, J.R., Koschinsky, A., Bau, M., Manheim, F.T., Kang, J.K., 1999. Cobalt-rich ferromanganese crusts in the Pacific. In: Handbook of Marine Mineral Deposits, pp. 239–279.
Isaaks, E.H., Srivastava, R.M., 1988. Spatial continuity measures for probabilistic and deterministic geostatistics. Math. Geol. 20 (4), 313–341.
Isaaks, E.H., Srivastava, R.M., 1989. An Introduction to Applied Geostatistics. Oxford University Press, New York, USA.
Iwashita, F., Monteiro, R.C., Landim, P.M., 2005. An alternative method for calculatingvariog ram surfaces using polar coordinates. Comput. Geosci. 31, 801–803.
Journel, A.G., 1987. Geostatistics for the Environmental Sciences: An Introduction. US Environmental Protection Agency, Environmental Monitoring Systems Laboratory.

Journel, A.G., 1988. New Distance Measures: The route toward truly nongaussian geostatistics. Math. Geol. 20 (4), 459–475.
Journel, A.G., 1989. Fundamentals of Geostatistics in Five Lessons, 8. American Geophysical Union, Washington, DC, pp. 2–8.
Journel, A.G., Huijbregts, C.J., 1978. Mining Geostatistics. Academic press Inc, London.
Krige, D.G., 1951. A statistical approach to some basic mine valuation problems on the witwatersland. J. Chem. Metallurgical Mining Soc. S. Afr. 94 (3), 95–111.
Lu, G.Y., Wong, D.W., 2008. An adaptive inverse-distance weighting spatial interpolation technique. Comput. Geosci. 34, 1044–1055.
Luenberger, D.G., 1969. Optimization by Vector Space Methods, 41(162). Wiley, pp. 228–229.
Nwankwoala, H.O., Eludoyin, O.S., Obafemi, A.A., 2012. Groundwater water quality assessment and monitoring using geographic information systems (GIS) in port Harcourt, Nigeria. Ethiopian J. Environ. Studies Manage. 5 (4), 583–596.
Olea, R.A., 1991. Geostatistical Glossary and Multilingual Dictionary, No. 3. Oxford University Press Inc, New York, p. 177.
Omre, H., 1984. The variogram and its estimation. In: Geostatistics for Natural Resources Characterization. Springer, Netherlands, pp. 107–125.
Soleimani, B., Nazari, K., Bakhtiar, H.A., Haghparast, G., 2008. Three-dimensional geostatistical modeling of oil reservoirs: a case study from the Ramin oil field in Iran. J. Appl. Sci. 8 (24), 4523–4532.
Usui, A., Someya, M., 1997. Distribution and composition of marine hydrogenetic and hydrothermal manganese deposits in the Northwest Pacific. Geol. Soc. London, Special Publications 119 (1), 177–198.
Zhang, F., Zhang, W., Zhu, K., Zhang, X., Zhu, B., 2008. Distribution characteristics of cobalt-rich ferromanganese crust resources on submarine seamounts in the Western Pacific. Acta Geol. Sinica 82 (4), 796–803.